The HKU Scholars Hub   The University of Hong Kong   香港大學學術庫

Title	X-Ray Analysis of the Proper Motion and Pulsar Wind Nebula for PSR J1741-2054
Author(s)	Auchettl, K; Slane, P; Romani, RW; Posselt, B; Pavlov, GG; Kargaltsev, O; Ng, SCY; Temim, T; Weisskopf, MC; Bykov, A; Swartz, DA
Citation	The Astrophysical Journal, 2015, v. 802, p. 68
Issued Date	2015
URL	http://hdl.handle.net/10722/209813
Rights	Creative Commons: Attribution 3.0 Hong Kong License

X-RAY ANALYSIS OF THE PROPER MOTION AND PULSAR WIND NEBULA FOR PSR J1741-2054

Katie Auchettl[1,2], Patrick Slane[1], Roger W. Romani[3], Bettina Posselt[4], George G. Pavlov[4], Oleg Kargaltsev[5],
C.-Y. Ng[6], Tea Temim[7,8], Martin. C. Weisskopf[9], Andrei Bykov[10], and Douglas A. Swartz[9]

[1] Harvard-Smithsonian Center for Astrophysics, 60 Garden Street, Cambridge, MA 02138, USA
[2] School of Physics & Astronomy, Monash University, Melbourne, Victoria 3800, Australia
[3] Department of Physics, Stanford University, Stanford, CA 94305, USA
[4] Department of Astronomy & Astrophysics, Pennsylvania State University, 525 Davey Lab, University Park, PA 16802, USA
[5] Department of Physics, The George Washington University, 725 21st St, NW, Washington, DC 20052, USA
[6] Department of Physics, The University of Hong Kong, Pokfulam Road, Hong Kong, China
[7] Observational Cosmology Lab, Code 665, NASA Goddard Space Flight Center, Greenbelt, MD 20771, USA
[8] CRESST, University of Maryland-College Park, College Park, MD 20742, USA
[9] NASA/Marshall Space Flight Center, ZP12, 320 Sparkman Drive, Huntsville, AL 35805, USA
[10] A.F. Ioffe Physical-Technical Institute, St. Petersburg 194021, also St.Petersburg State Politechnical University, Russia

ABSTRACT

We obtained six observations of PSR J1741-2054 using the *Chandra* ACIS-S detector totaling $\sim$300 ks. By registering this new epoch of observations to an archival observation taken 3.2 yr earlier using X-ray point sources in the field of view, we have measured the pulsar proper motion at $\mu = 109 \pm 10$ mas yr^{-1} in a direction consistent with the symmetry axis of the observed Hα nebula. We investigated the inferred past trajectory of the pulsar but find no compelling association with OB associations in which the progenitor may have originated. We confirm previous measurements of the pulsar spectrum as an absorbed power law with photon index $\Gamma = 2.68 \pm 0.04$, plus a blackbody with an emission radius of $(4.5^{+3.2}_{-2.5})d_{0.38}$ km, for a DM-estimated distance of $0.38d_{0.38}$ kpc and a temperature of 61.7 ± 3.0 eV. Emission from the compact nebula is well described by an absorbed power law model with a photon index of $\Gamma = 1.67 \pm 0.06$, while the diffuse emission seen as a trail extending northeast of the pulsar shows no evidence of synchrotron cooling. We also applied image deconvolution techniques to search for small-scale structures in the immediate vicinity of the pulsar, but found no conclusive evidence for such structures.

Key words: pulsars: individual (PSR J1741-2054) – X-rays: general

1. INTRODUCTION

PSR J1741−2054 (J1741) is one of the closest middle-aged ($\tau_c = 390$ kyr) pulsars known. It has a period of $P = 413$ ms and was first discovered in γ-rays using the Large Area Telescope (LAT) on the *Fermi Gamma-ray Space Telescope* by a blind search for periodic γ-ray pulsations from Fermi-LAT point sources (Abdo 2009). It was subsequently detected in archival Parkes radio data and observed using the Green Bank Telescope (Camilo et al. 2009). The pulsar has a spin-down energy loss rate of $\dot{E} = 9.5 \times 10^{33}$ erg s^{-1} which is moderately low compared to those of other γ-ray pulsars. The pulsar has a very small dispersion measure (DM) = 4.7 pc cm^{-3} and a magnetic field of 2.7×10^{12} G. Using the NE2001 Galactic electron density model, the low DM implies a distance of 0.38 kpc (Cordes & Lazio 2002). At this distance, its measured radio flux at 1400 MHz ($S \sim 160\,\mu$Jy) makes it one of the least luminous radio pulsars known. Its γ-ray pulsations lag behind its radio pulsations by $\delta = 0.29\,P$, implying that our line of sight tangentially cuts the γ-ray cone, while nearly missing the radio beam (Camilo et al. 2009). This makes J1741 a transitional object between a classical radio/γ-ray loud pulsar such as Vela and the radio-quiet Geminga-type pulsars. Interestingly, Romani et al. (2010) detected a 20″ long, non-radiative Hα bow shock nebula around the pulsar. Modeling of the bow shock suggested that the pulsar is traveling with a velocity of $\sim$150 km s^{-1}, while the observation of negative radial velocities from both sides of the nebula imply that the velocity is directed out of the plane of the sky at an angle of $15° \pm 10°$.

Using a short *Chandra* ACIS-S observation (observation ID (ObsID): 11251), Romani et al. (2010) detected an X-ray pulsar wind nebula (PWN) within this Hα nebula and a long (>2 arcmin) X-ray trail at an angle of $45° \pm 5°$ east from north. Romani et al. (2010) also suggested that there are asymmetries in the small scale structure surrounding the pulsar, which they associate with a compact 2.″5 equatorial toroidal structure. Marelli et al. (2014) and Karpova et al. (2014) performed a spectral analysis of the pulsar emission using *XMM-Newton* and *Chandra* and determined that a two-component (blackbody plus power-law) model is required to obtain satisfactory spectral fits.

In this paper, we use $\sim$300 ks of *Chandra* data of J1741 that were obtained as part of the Cycle 14 *Chandra* Visionary Project "A Legacy Study of the Relativistic Shocks of PWNe," plus a $\sim$49 ks archival observation, to constrain the pulsar motion, and the geometry of the PWN outflow. We discuss our approach to image registration and proper motion measurement in Section 3, followed by a discussion in Section 4 of our image deconvolution efforts to search for small-scale structure around the pulsar. In Section 5 we discuss the results of our spectral fits for the pulsar emission and that of the extended PWN, and compare these with previous results. In Section 6 we discuss the implications of the proper motion measurements, including comparisons with the observed Hα nebula surrounding J1741, and discuss the lack of evidence of for synchrotron cooling in the PWN trail. Our conclusions are summarized in Section 7.

Table 1
Chandra Observations of PSR J1741-2054

Observation ID	Exposure Time (ks)	Observation Date
Archival	…	…
11251	48.78	2010-05-21
New observations	…	…
14695	57.15	2013-02-06
14696	54.30	2013-02-19
15542	28.29	2013-04-01
15638	29.36	2013-04-02
15543	57.22	2013-05-15
15544	55.73	2013-07-09

2. X-RAY DATA ANALYSIS

We obtained 282 ks of new *Chandra* ACIS-S exposure time of J1741. Table 1 lists the parameters for each of the six new observations that we obtained, including the archival observation. To reduce pileup, the CCDs were operated in half-frame VFAINT mode so that events were read out every 1.7 s. The pulsar was placed near the optimum focus on the backside illuminated S3 chip. In addition to our six observations, there is a 48.8 ks archival observation (ObsID: 11251), which was taken on 2010 May 21. Each new observation has a roll angle similar to the roll angle of the 2010 epoch ($\sim90°$), except for ObsID: 15544. This observation has a roll angle of $\sim260°$ as the nominal roll angle of *Chandra* is rotated by 180° during the time of the year this observation was completed. The data were analysed with *CIAO* 4.6.2 after all observations were reprocessed using the CALDB 4.5.9. No flaring occurred in any of the observations so the full exposure times were used.

Using all seven observations we produced a merged, exposure-corrected image of J1741 by reprojecting the new observations to a common tangent plane based on the WCS information of ObsID: 11251 (*CIAO* task: *reproject_obs*) and combined all reprojected observations into an exposure corrected image using the *CIAO* task *flux_obs*. The merged ACIS-S image of the extended emission around the pulsar, smoothed with a 3″ Gaussian, is shown in Figure 1. The pulsar point source lies at the apex of the diffuse X-ray emission, while a diffuse, faint X-ray trail extending $\sim1'.9$ is seen toward the northeast of the pulsar.

3. REGISTRATION AND THE PROPER MOTION

To constrain the proper motion of the pulsar, we registered each of the new *Chandra* images to the archival image using field point sources that were identified using the *CIAO* tool *wavdetect*. We selected sources with a detection significance of $>3\sigma$ that were found on the S3 chip in both the 2010 observation and the corresponding new observation. These sources are highlighted in white and the pulsar is labeled as *P* in Figure 1.

Careful consideration and modeling of the point-spread function (PSF) must be undertaken to reduce the effect of changes in the PSF shape on the count distribution of our point-sources. To improve the astrometric accuracy and reduce this effect, we simulate a PSF for each point source position, in each observation, and use it to fit for the position of the source.

To simulate a PSF of a point source, we use the software suite *SAOTrace*[11] which is designed to simulate the propagation of photons from astronomical objects through the optics of the *Chandra* X-ray satellite. We use the aspect solution file of each observation and provided spectral information for the ray trace by extracting the spectrum of each stellar source using the *CIAO* task *specextract*. We model the spectra using an absorbed Mekal model in *SHERPA*. To improve the accuracy of the PSF modeling, we increase the normalization of this spectrum by a factor of 100 before passing it into *SAOTrace*. A model of a point source at its position is obtained by passing the raytrace from *SAOTrace* into the program MARX.[12] Each PSF model is corrected for the science instrument module (SIM) offset from nominal location and filtered using the Good Time Interval data from the original event file.

To determine the position of the sources we use the maximum likelihood "figure of merit" (FoM) technique developed by van Etten et al. (2012). We generate a 39 pixel by 39 pixel image of the modeled PSF, binned to 1/9 ACIS pixel resolution. This is then compared to 0.3–5.0 keV source images of the same size but binned to native ACIS pixel resolution. PSF models and source images are produced for all observations and for each registration source. The PSF is shifted along the x and y axes of the 1/9 pixel grid and rebinned to native ACIS pixels. We then compute the FoM at each offset in pixel coordinates, giving us a map of the likelihood of the observed counts with respect to the x and y position. To determine the best-fit position of the source, we fit a two-dimensional Gaussian to the FoM surface, with the minimum of this surface providing the best fit position of the source. The standard deviations along x and y are estimated by calculating the square root of the eigenvalues of the covariance matrix.

Prior to registration we checked each source for any optical counterparts using VizieR.[13] Sources 6, 8, 9, 10 and 13 all have optical counterparts within 2″ of the PSF-fit position. Source 8 and 13 have estimated proper motions of $(\mu_{R.A.}, \mu_{Decl.}) = (22, -62)$ mas yr^{-1} and $(20, -22)$ mas yr^{-1}, respectively (errors $\delta\mu_{R.A.} \sim 7$ mas yr^{-1}, $\delta\mu_{Decl.} \sim 15$ mas yr^{-1}). We corrected for these nominal proper motions, but also confirmed that our final astrometric solution was insignificantly changed if we excluded these two stars from the analysis.

Using the FoM positions of our registration sources and their uncertainties as a reference grid to perform the relative astrometry, we determined the best translation transformation needed to register the images from the two epochs using the *CIAO* command *wcs_match*. For each observation we adopt the *Chandra*-determined roll angle. In Table 2 we list the best-fit frame shifts and their uncertainties. The uncertainties in these shifts were calculated by adding in quadrature the errors in the differences between each source before and after shift. Adding a rotation to the transformation did not produce a statistically significant improvement on the best-fit translation.
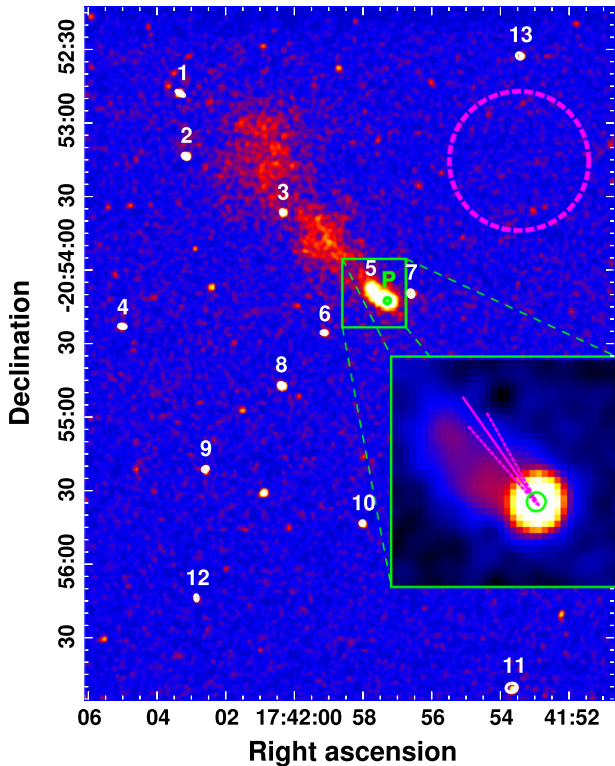
To calculate the position of the pulsar after registration, we first calculate the position of the pulsar in the unregistered frames. We simulate a PSF at the position of the pulsar in each observation using the method described for the registration sources. To define the energy dependence of the PSF, we extract a spectrum of the pulsar and fit it with an absorbed

---

[11] http://cxcoptics.cfa.harvard.edu/SAOTrace/Index.html
[12] http://space.mit.edu/CXC/MARX/
[13] http://vizier.u-strasbg.fr/viz-bin/VizieR

Figure 1. Merged *Chandra* exposure-corrected 0.3–5.0 keV ACIS-S image of the extended emission around J1741-2051. This was produced using *reproject_obs* and *flux_obs* and incorporates all available *Chandra* observations. The image is smoothed using a Gaussian of width 3″ and plotted on the logarithmic scale. The reference sources numbered 1 through 13 were used for relative astrometry, while the pulsar is labeled as *P*. Other sources seen in the image are not suitable for astrometry because, being variable, they were not significantly detected in both the archival observation and one of the new epoch observations. We included a cutout region around the pulsar to show the point source. The magenta lines show our derived proper motion (solid) and its uncertainty (dashed), traced back from the pulsar position. The background region used for spectral analysis is shown as the magenta dashed circle.

Table 2
Frame Shifts and Their Uncertainties Used for Registration

ObsID	R.A. (arcsec)	Decl. (arcsec)
14695	-0.02 ± 0.02	0.48 ± 0.02
14696	-0.01 ± 0.02	0.25 ± 0.02
15542	0.02 ± 0.04	0.43 ± 0.04
15638	-0.06 ± 0.03	0.36 ± 0.03
15543	0.23 ± 0.02	0.29 ± 0.03
15544	-0.11 ± 0.03	-0.29 ± 0.03

power law plus blackbody model (see Section 5). For each observation, we generate a 6 pixel by 6 pixel image of the PSF model of the pulsar that is binned to 1/4 ACIS pixel resolution. Using an image of the 0.3–5.0 keV pulsar events of the same size and binning, we fit for the position of the pulsar in *SHERPA*. In this fit, we used a delta function (the pulsar) plus a two-dimensional Gaussian (the circumpulsar PWN), both convolved with the PSF. The resulting pulsar fit position for each frame was then registered by applying the best-fit transformations (Table 2).

To quantify the proper motion of the pulsar, we plot in Figure 2 the offset in the position of the pulsar between the archival observation and the new observations against the number of years since the archival observation. The uncertainties in the offset are calculated by adding in quadrature the uncertainties in the fit positions of the pulsar, the uncertainty in the frame shifts and the systematic uncertainty associated with choosing a particular tangent plane when creating an image in sky coordinates. We fit the offset using a linear function that corresponds to the positional shift of the pulsar between the archival observation and the new observations and this is seen as the dashed line in Figure 2.

We obtain a proper motion of $\mu_{\mathrm{R.A.}} \cos(\delta) = -63 \pm 12$ mas yr^{-1} and $\mu_{\mathrm{Decl.}} = 89 \pm 9$ mas yr^{-1}. This corresponds to a total proper motion of 109 ± 10 mas yr^{-1}. Assuming a distance of 0.38 kpc to the pulsar, this translates to a transverse velocity of $(196 \pm 18)d_{0.38}$ km s^{-1}. The position angle of the proper motion is $215° \pm 6°$ east of north. The proper motion axis points in the opposite direction of the extended X-ray trail as expected (see Figure 1).

4. X-RAY IMAGING

Using the archival *Chandra* observation of J1741 (ObsID: 11251), Romani et al. (2010) performed a PSF subtraction of the pulsar point source to look for any small-scale structure surrounding the pulsar. They discovered that the region around the pulsar appears to be slightly extended and they associate this feature with the equatorial torus of the PWN. Using the same data as analyzed here, Karpova et al. (2014) searched for evidence of such structure by performing fits to a two-dimensional Gaussian convolved with PSF models generated for each observation. They found no evidence for any small-scale extended features other than for a small emission feature associated with a known mirror artifact.[14] We have carried out a similar investigation using image deconvolution techniques. We simulate a PSF of the pulsar in each observation using MARX following re-reduction of our *Chandra* observations with CALDB 4.4.7 to match the calibration data used for MARX. We define the energy dependence of the PSF as described in Section 3 and use the dither pattern of the observation with an aspect blur of 0.07, which corresponds to the uncertainty in the telescope pointing.[15] We also correct for SIM offset. Using this PSF we deconvolve a 0.3–5.0 keV pulsar image using the Lucy–Richardson deconvolution algorithm (Lucy 1974) implemented using the *CIAO* task *arestore*. All images were binned to quarter-ACIS pixel. We ran *arestore* multiple times using a number of different iterations between 10 and 200 to determine convergence of new features. No new structures appeared after 50 iterations.

The deconvolved image from one observation is shown in Figure 3. The emission is well described by a point source, with the exception of the artifact feature (identified in cyan). We thus see no conclusive evidence of other small-scale structure in the immediate region surrounding the pulsar, consistent with the results reported by Karpova et al. (2014).

---

[14] http://cxc.harvard.edu/ciao/caveats/psf_artifact.html
[15] http://space.mit.edu/CXC/marx/news.html
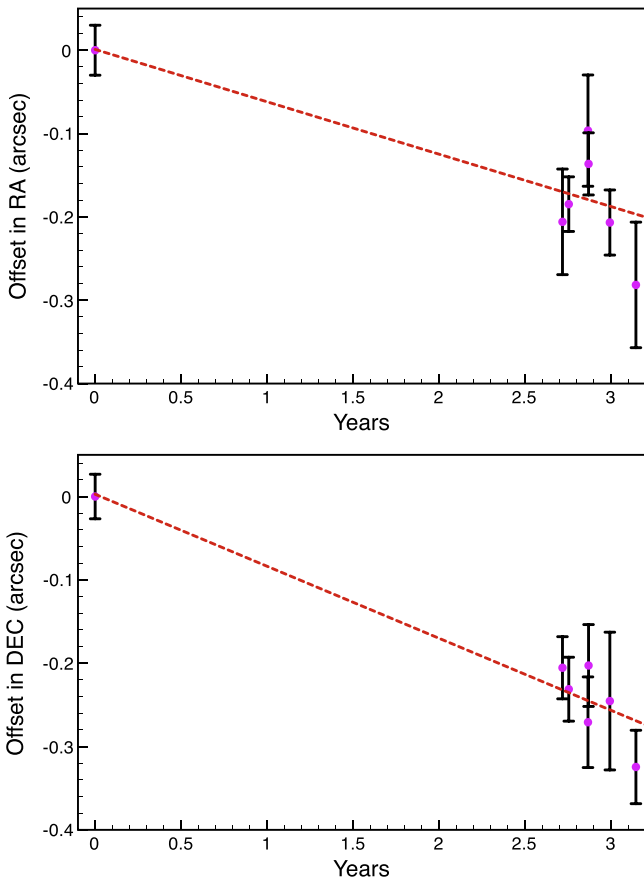
Figure 2. Offset in the position of the pulsar in R.A. (top) and decl. (bottom) in the new observations from the position of the pulsar in the archival observation plotted against the time since the first observation of PSR J1741 with *Chandra* (years). The dashed line corresponds to the line of best fit in which the slope corresponds to the proper motion of the pulsar.
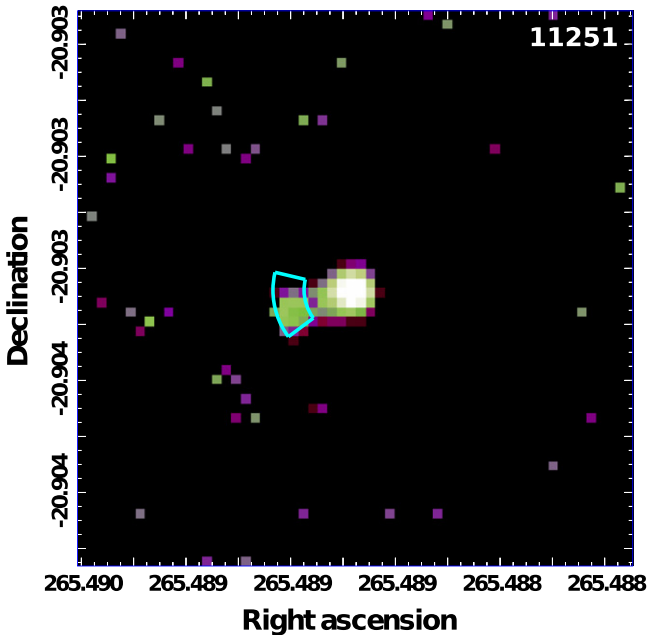
Figure 3. Deconvolved image of J1741-2054 from ObsID 11251 obtained using *arestore* after 50 iterations. The cyan region corresponds to the PSF asymmetry seen in *Chandra* data when pushing to sub-ACIS-pixel resolution. The image has been logarithmically stretched and the color enhanced to highlight the observed features.

5. SPECTRAL ANALYSIS OF THE X-RAY EMISSION OF THE PULSAR AND ITS TRAIL

5.1. Pulsar

As noted above, modeling of the *Chandra* PSF for use in determining an accurate pulsar position requires knowledge of the source spectrum. *XMM-Newton* observations establish a two-component spectrum for the pulsar, with a blackbody accompanied by a power law (Marelli et al. 2014). Similar results were derived by Karpova et al. (2014) using the same *Chandra* data reported here. We have re-analyzed these data by extracting events from a 0″.70 radius region centered on the pulsar, shown as the green circle in Figure 4(a). The size of this region was chosen to minimise the contamination from the PWN, and subsequent modeling results have been corrected for the finite encircled energy fraction. All spectra were grouped with a minimum of 20 counts per bin, and a background spectrum was obtained using a source-free circular region with a radius of 30″, as shown by the magenta circle in Figure 1. Using the *CIAO pileup_map*, we determined that approximately 5% of the pulsar events suffer from pileup. We thus included a pileup model in our spectral fits, where the frame time is 1.7 s and the PSF fraction is allowed to vary. All other parameters in the pileup model were frozen at default values.

To constrain the column density, we fit spectra from the compact nebula to the northeast of the pulsar (see Section 5.2) using an absorbed power law (more details in Section 5.2). We obtained $N_H = (1.20^{+0.08}_{-0.07}) \times 10^{21}$ cm^{-2}, in good agreement with the above studies, and adopt this value in all our models of the pulsar spectrum. We use the Wilms et al. abundance table throughout our analysis (Wilms et al. 2000). Modeling the spectrum with a power-law plus blackbody model, we obtained a photon index of $\Gamma = 2.68 \pm 0.04$ and a blackbody spectrum with a temperature of $kT_{eff} = 61.7 \pm 3.0$ eV, in excellent agreement with the results reported by Marelli et al. 2014 and Karpova et al. (2014). Omitting the pile-up correction yields similar values. We use the best-fit values above for PSF modeling of the pulsar.

We also ran fits using magnetized neutron star atmosphere models (*nsa* and *nsmax* in *SHERPA*) for the thermal component. These gave somewhat different temperatures and emitting areas, but did not significantly improve the quality of the fit. For example a magnetic carbon atmosphere model (*nsmax* model 12006, Mori & Ho (2007)) gave a temperature of $kT_{eff} = 86.0 \pm 9.0$ eV and emission radius of $R_{emis} = (4.90^{+3.0}_{-2.3}) d_{0.38}$ km. The power law component was only slightly affected with $\Gamma = 2.63 \pm 0.03$.

5.2. PWN and its Extended X-ray Trail

To analyse the spectrum of the compact nebula described above, we extracted spectra from each observation using the cyan rectangular region in Figure 4(a) and combined these using *specextract*. We used the same background spectrum as for the pulsar spectrum. The compact nebula contains a total of ~900 counts and we binned the combined spectrum with a minimum of 20 counts per spectral bin. The PWN spectrum is consistent with an absorbed power law with an index of $\Gamma = 1.60 \pm 0.20$.

To determine whether there is any spectral variation in the PWN and its extended trail, we extract spectra from the five regions defined in Figure 4(b). These regions correspond to roughly the same spectral regions reported by Marelli et al.
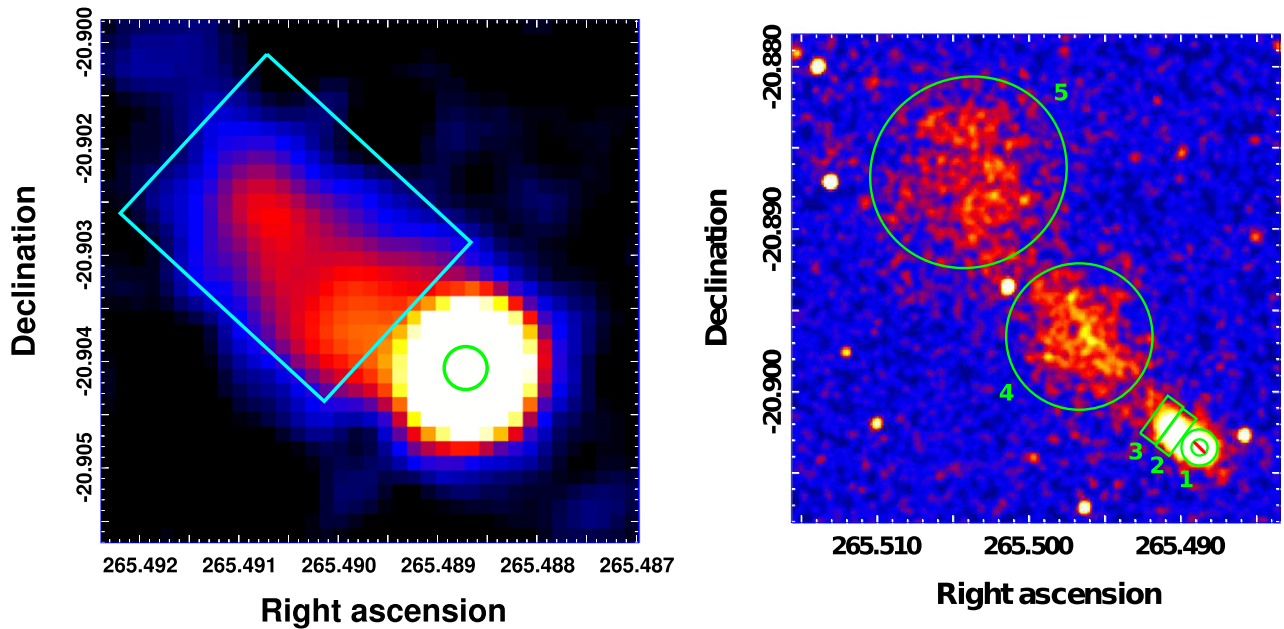
Figure 4. Logarithmically scaled, merged *Chandra* exposure-corrected 0.3–5.0 keV ACIS-S image of the pulsar and its extended emission. Left: the green circular region defines the 0″70 region used to extract the spectrum of the pulsar from all available observations. The cyan rectangular region defines the region used to extract the spectrum of the pulsar's compact nebula from all observations. Right: the green regions define the apertures used to look for spectral variability in the extended emission of the pulsar. The pulsar was excluded from the spectral extraction of region 1.

Table 3
Spectral Fit Values of the Extended Emission of the Pulsar Defined by the Cyan Colored Region in Figure 4(a) and the Green Regions Defined in Figure 4(b)

Region	$N_H (\times 10^{21})$ cm^{-2a}	Γ	Absorbed Flux 10^{-14} erg cm^{-2} s^{-1}	Unabsorbed Flux 10^{-14} erg cm^{-2} s^{-1}	χ^2/dof
Compact PWN	$1.20^{+0.08}_{-0.07}$	1.60 ± 0.20	$2.86^{+0.17}_{-0.20}$	$3.15^{+0.09}_{-0.07}$	0.90
1	⋯	$1.97^{+0.18}_{-0.17}$	$1.56^{+0.13}_{-0.12}$	1.81 ± 0.33	0.99
2	⋯	$1.50^{+0.16}_{-0.15}$	$1.54^{+0.15}_{-0.10}$	1.67 ± 0.16	0.84
3	⋯	$1.57^{+0.20}_{-0.19}$	$0.81^{+0.08}_{-0.11}$	1.10 ± 0.11	0.80
4	⋯	$1.63^{+0.12}_{-0.11}$	$4.35^{+0.28}_{-0.15}$	$4.81^{+0.04}_{-0.14}$	0.99
5	⋯	$1.70^{+0.10}_{-0.11}$	$5.40^{+0.29}_{-0.36}$	$6.03^{+0.06}_{-0.16}$	1.16

Note. All uncertainties are one σ.
[a] Fixed at value from joint compact nebula.

(2014), except that we investigate smaller regions in the compact nebula near the pulsar. In the outer portions of the nebula, the count rate is too low to obtain good spectra in smaller regions. We model each region individually using an absorbed power law, where we fix column density to the value derived earlier from fits to the inner nebula region but let photon index and the normalization vary. We have listed in Table 3 the absorbed flux, unabsorbed flux and the reduced χ^2 for each region, as well as the best-fit parameters from fitting the trail spectra. There is no evidence of systematic variation in the photon index of the compact nebula and trail (regions 1–5). The photon index of region 1 is slightly higher than that of the other four regions, but is consistent within uncertainties with all regions except for region 2. This slight variation between region 1 and 2 could suggest that region 1 is affected by leakage of the softer emission from the point source. Modeling the photon index as a function of distance from the pulsar using a linear regression fit with a constant function in *SHERPA*, we obtain $\Gamma = 1.67 \pm 0.06$ for the trail. The global PWN index derived from the *SHERPA* fit and the values we obtained in Table 3 are consistent with Karpova et al. (2014) and Marelli

et al. (2014), who derived $\Gamma = 1.74 \pm 0.07$ and $\Gamma = 1.78 \pm 0.15$ respectively for the PWN.

6. DISCUSSION

Using *Chandra* observations of PSR J1741-2054 that span a ∼3.2 yr period, relative astrometry measurements have identified a proper motion of $\mu = 109 \pm 10$ mas yr^{-1}. This corresponds to a modest velocity of $(196 \pm 18) d_{0.38}$ km s^{-1}, which agrees well with the velocity derived by Romani et al. (2010) using Hα spectroscopy. The larger distance of Karpova et al. (2014) gives a transverse velocity of ∼400 km s^{-1}, inconsistent with that obtained from optical spectroscopy. The direction of the proper motion is $205° \pm 6°$ east of north, opposite the elongated X-ray trail. Ng & Romani (2004); Johnston et al. (2005) and Ng & Romani (2007) found that the direction of proper motion of a pulsar is, generally, approximately parallel to its rotation axis.

In Figure 5 we plot the pulsar track (red) in Galactic coordinates (note the expanded *b* scale). This has the pulsar skimming above the plane. It does not intersect the plane itself unless one extrapolates an unreasonable ∼2 × 10⁶ yr;
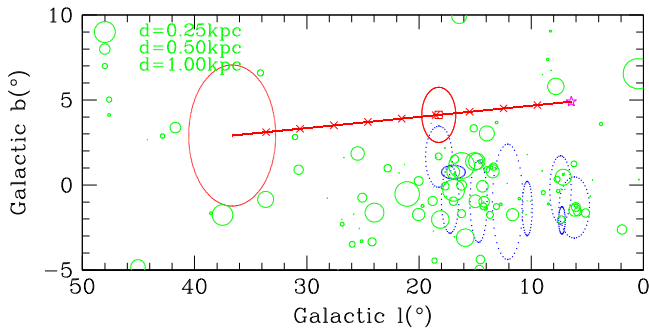
Figure 5. The past trajectory (red) of PSR J1741-2051 in Galactic coordinates. Positions are marked every 10^5 yr, with uncertainty ellipses at $\tau_c = 3.91 \times 10^5$ yr and at 10^6 yr. For comparison we show the locations and sizes of OB associations from the Mel'Nik & Efremov (1995) catalog (blue dotted ellipses) and the *Hipparcos* sample of OB stars (green circles). A substantial concentration of OB stars at $\sim 0.3-0.6$ kpc lies near the pulsar track at $\sim \tau_c$ and a more distant ($d = 1.45$ kpc) OB association overlaps with the track uncertainty at this age.

however, the track starts within the ~ 50 pc OB star scale height for $t \sim \tau_c$ and distances $d < 1$ kpc. For comparison we plot the positions of the *Hipparcos* catalog OB stars (green), with circle size proportional to the parallax. This set is quite complete, with useful parallaxes, to ~ 500 pc, and increasingly incomplete at larger distances. At large distance the cataloged OB associations (Mel'Nik & Efremov 1995) provide plausible pulsar birthsites, and their cataloged extent is plotted by the blue dotted ellipses. Intriguingly, one association overlaps the pulsar track, but this is at a likely unreasonable catalog distance of 1.45 kpc. We conclude that, with the pulsar motion passing along the Galactic plane, there will be many superposed massive star locations, and no definitive birthsite can be identified. However, there are certainly many plausibly associated massive stars consistent with our preferred $d \sim 0.4$ kpc, especially considering that some pulsar progenitors may be OB runaways with significant offset during their pre-explosion lifetime.

Neither our deconvolved nor our PSF-subtracted images indicate conclusive evidence of small-scale structure surrounding the pulsar that might be associated with a torus or jet-like feature. The equatorial torus structure that Romani et al. (2010) associate with a diagonal excess seen $\sim 0\farcs75$ from the core of the pulsar image seems to have arisen from the mirror asymmetry. Karpova et al. (2014) perform a similar analysis and come to the same conclusion. However, it is interesting to compare the nebula head and proper motion with the Hα structure described in Romani et al. (2010). In Figure 6 we see that the pulsar lies very close to the bow shock limb (accuracy limited by our relative X-ray/optical astrometry). Interestingly, our measured proper motion is consistent with, although nominally slightly south of, the Hα nebula's symmetry axis. However the X-ray PWN trail fills only the southern half of the apparent Hα cavity, punching out through a gap at the back end of the Hα emission and continuing to the arcmin-scale trail beyond. The origin of this asymmetry is unclear, but a clue may be seen in the X-ray contours, whose ridge line lies at PA $\approx 70°$, i.e., misaligned with the proper motion by $\approx 35°$. This suggests a second symmetry axis in the PWN, possibly due to a pulsar jet or other outflow concentration. This directs the shocked PWN plasma to the southeast, preferentially filling this half of the Hα cavity. A more complete discussion of the PWN geometry, including the 3D Hα kinematics, is in preparation.

The X-ray spectrum of the pulsar requires a combination of non-thermal and thermal model components. The emission is dominated by the non-thermal component ($\sim 75\%$ of unabsorbed flux), indicating that the majority of the X-ray emission is magnetospheric in nature. The emitting radius implied by the blackbody model for J1741 corresponds to $(4.5^{+3.2}_{-2.5})d_{0.38}$ km. This is substantially smaller than any viable neutron star radius (Lattimer & Prakash 2007), suggesting that this thermal emission arises from hot spots on the surface, plausibly near the magnetic poles (Ho & Heinke 2009). In fact, Marelli et al. (2014) do detect a pulsed thermal component for PSR J1741, also supporting such a surface temperature inhomogeneity.

The X-ray emission from the compact nebula and the trail is consistent with an absorbed power law. There is no discernible evidence of spectral variation with distance from the pulsar and the spectrum of the entire tail can be described by $\Gamma = 1.67 \pm 0.06$. We compute the minimum (equipartition) energy by approximating the X-ray emission from the PWN (region 2, 3, 4 and 5 in Figure 4(b)) as a cylinder with length $l \sim 108$ arcsec $(0.20 d_{0.38}$ pc) and width $w \sim 18$ arcsec $(0.03 d_{0.38}$ pc), comprising a volume of $V \sim 5.0 \times 10^{51} \phi d^3_{0.38}$ cm^3, where ϕ is filling factor. The minimum energy in relativistic particles and magnetic field required to produce a synchrotron source of a given luminosity (Pacholczyk 1970) yield $E_{\min} \sim C(1 + \kappa)^{4/7} V^{3/7} L_{\rm syn}^{4/7}$, where κ is the ion to electron energy ratio, $L_{\rm syn}$ is the synchrotron luminosity and C is a function dependent on energy, electron charge, speed of light and the mass of the electron in Gaussian cgs units (see Pacholczyk 1970). In the following, we considering only the leptonic case, where $\kappa = 0$. The total luminosity of the PWN is $L(0.5-10.0\,{\rm keV}) = 2.36 \times 10^{30}$ erg s^{-1}, giving $E_{\min} \sim 5.50 \times 10^{40} \phi^{3/7} d^{17/7}_{0.38}$ erg. The associated minimum-energy magnetic field is $B_{\min} \sim (D(1 + \kappa) L_{\rm syn})^{2/7} V^{-2/7}$, where D is a function similar to C. This magnetic field is $\sim 15 \phi^{-2/7} d^{-2/7}_{0.38} \mu$ G, leading to a lifetime of the X-ray emitting leptons of $\tau_{\rm syn} \sim 6.4 \times 10^4 B_{\mu \rm G}^{3/2} E_{\rm keV}^{-1/2}$ yr or ~ 1100 yr at an observed photon energy of 1 keV. This is comparable to the (length/proper motion) $= 108''/109 \sim 10^3$ yr required for the pulsar to traverse the bright trail with our observed proper motion. Thus it is not surprising that there is no dramatic spectral steeping along the trail. If the PWN electrons flow at even faster speeds within the trail, this conclusion is even stronger.

7. CONCLUSION

Using ~ 300 ks of *Chandra* ACIS-S observations of PSR J1741-2054, we were able to determine the proper motion of the pulsar with a detection significance $> 3\sigma$. The direction of the proper motion is aligned with the extended PWN emission, and corresponds well with a symmetry axis of the associated Hα nebula. The diffuse X-ray emission immediately behind the pulsar is concentrated in the southeastern portion of the Hα nebula, possibly suggesting another flow axis from a jet or torus in the pulsar system. The trajectory of the pulsar, extrapolated over the characteristic age, does not provide a compelling correlation with known OB associations at the distance of the pulsar, although there are many massive stars consistent with this distance that could potentially have had a common origin.

The pulsar spectrum is well described by an absorbed power law accompanied by a blackbody with an emission radius of
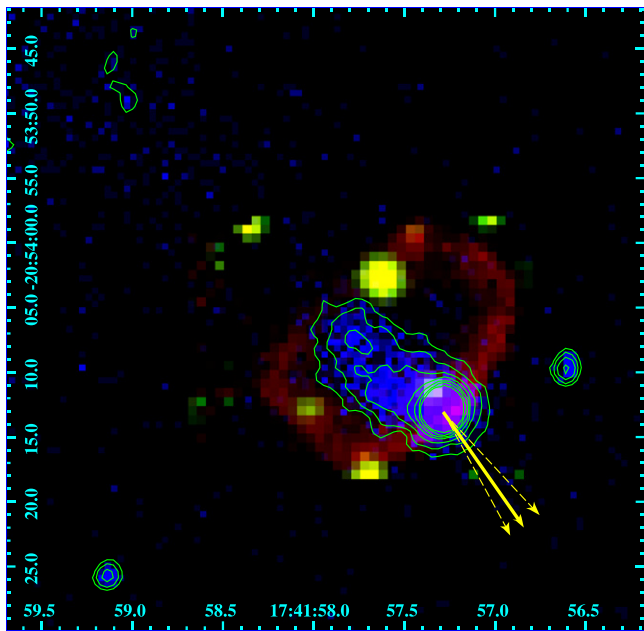
Figure 6. The head of the PSR J1741-2051 nebula. The red channel shows Hα emission at $6562-6564$ Å while the green channel shows the average of the continuum $6551-6561, 6565-6575$ Å with data abstracted from an AAT SPIRAL IFU observation. The blue channel shows the $0.3-7$ keV X-ray photons from our combined new observation. Green contours help one to read the X-ray structure, while the yellow arrows show our measured proper motion, with the arrow heads marking the position in 100 yr.

$(4.5^{+3.2}_{-2.5})d_{0.38}$ km and a temperature of $kT_{\mathrm{eff}} = 61.7 \pm 3.0$ eV, as found in earlier works. The thermal component, a hot region on the neutron star surface, is augmented by a magnetospheric

or unresolved PWN power law component. The PWN plus its extended trail can be well described using an absorbed power law and there is no evidence of variation in the photon index with distance from the pulsar. The integrated luminosity of the PWN over the $0.5-10$ keV is 2.36×10^{30} erg s^{-1}. This represents 0.02% of the pulsar spin down power, which is not atypical. We find no conclusive evidence of small-scale structure surrounding the pulsar that we can associate with a torus or jet-like structure.

REFERENCES

Abdo, A. A. e. a. 2009, Sci, 325, 840
Camilo, F., Ray, P. S., Ransom, S. M., et al. 2009, ApJ, 705, 1
Cordes, J. M., & Lazio, T. J. W. 2002, arXiv:astro-ph/0207156
Ho, W. C. G., & Heinke, C. O. 2009, Natur, 462, 71
Johnston, S., Hobbs, G., Vigeland, S., et al. 2005, MNRAS, 364, 1397
Karpova, A., Danilenko, A., Shibanov, Y., Shternin, P., & Zyuzin, D. 2014, ApJ, 789, 97
Lattimer, J. M., & Prakash, M. 2007, PhR, 442, 109
Lucy, L. B. 1974, AJ, 79, 745
Marelli, M., Belfiore, A., Saz Parkinson, P., et al. 2014, ApJ, 790, 51
Mel'Nik, A. M., & Efremov, Y. N. 1995, AstL, 21, 10
Mori, K., & Ho, W. C. G. 2007, MNRAS, 377, 905
Ng, C.-Y., & Romani, R. W. 2004, ApJ, 601, 479
Ng, C.-Y., & Romani, R. W. 2007, ApJ, 660, 1357
Pacholczyk, A. G. 1970, Radio Astrophysics. Nonthermal Processes in Galactic and Extragalatic Sources, ed. G. Burbidge, & M. Burbidge (San Francisco, CA: Freeman)
Romani, R. W., Shaw, M. S., Camilo, F., Cotter, G., & Sivakoff, G. R. 2010, ApJ, 724, 908
van Etten, A., Romani, R. W., & Ng, C.-Y. 2012, ApJ, 755, 151
Wilms, J., Allen, A., & McCray, R. 2000, ApJ, 542, 914